CHAPTER 108

LAMINAR BOUNDARY LAYER AROUND A CIRCULAR CYLINDER UNDER OSCILLATORY WAVES

Yuichi Iwagaki Professor

and

Hajime Ishida Graduate Student

Department of Civil Engineering Kyoto University Kyoto, Japan

ABSTRACT

A solution of water particle velocities in the boundary layer developed by monochromatic waves on the surface of a circular cylinder is obtained by applying the boundary layer approximations and perturbation method to the Navier-Stokes and continuity equations represented in the cylindrical coordinates. Since, in this process, it is necessary to give the velocity outside the boundary layer, the water particle velocities of diffracted waves around the cylinder are derived from MacCamy-Fuchs' velocity potential. Moreover, the occurrence of laminar flow separation is explained by using this solution.

On the other hand, using a hydrogen bubble tracer some experiments have been performed about the water particle velocities of diffracted waves, velocity profiles in the boundary layer and occurrence of wake vortices. These results are compared with theoretical ones.

INTRODUCTION

In estimation of the wave force on a circular cylinder, the Morison equation expressed as the sum of the inertia and drag forces is generally used. However, concerning the mechanism how the drag force is induced by wave motions, few papers have been reported yet, and therefore, it is right to say that the relationship between the drag coefficients under wave motion and in steady state flow is not clear yet.

On the other hand, in the diffraction theory presented by MacCamy and Fuchs¹⁾ to estimate the wave force on a large-diameter pile, since the drag force due to flow separation and subsequent vortex formation can not be contained because of neglecting the viscosity of the fluid, an applicable range of their theory is limited.

Therefore, in order to estimate the wave force more correctly, it is necessary to make progress in the study based on an idea of making clear the interaction between waves and the pile, that is, investigating the effect of the pile on the waves, and next, making clear the internal mechanism of the affected waves, and finally, evaluating the force on the pile in such velocity and pressure fields. From this viewpoint, the present study deals with the laminar boundary layer on the surface of a circular cylinder developed by monochromatic waves. The concept of boundary layer was introduced by Prandtl in 1904, and studies of the laminar flow around a circular cylinder in steady state have been made by Blasius, Karman, Hiementz, Porlhausen, Howarth and many other investigators. As a result, a lot of important facts were found about separation point, pressure distribution, characteristics of the drag coefficient and so on²⁾, ³. With respect to the laminar boundary layer on an oscillating circular cylinder in still water, Schlichting solved the boundary layer equation using successive approximations, and explained the existence of mass transport velocity outside the boundary layer³.

On the other hand, Keulegan and Carpenter investigated experimentally the relationship between the flow pattern around a horizontal cylinder installed under the nodal area of standing waves and the wave force acting on the cylinder, and found that the case when Keulegan-Carpenter's number is equal to 15 is a critical condition yielding the lowest value of the inertia coefficient and the largest value of the drag coefficient⁴⁾. The authors also investigated variations of the drag and inertia coefficients with Keulegan-Carpenter's number for progressive waves⁵⁾. However, these are not mentioned in this paper.

THEORY

The coordinate system is shown in <u>Fig.1</u>, in which (θ, \hbar, z) and (x, y, z) denote the cylindrical coordinates and boundary layer coordinates respectively.

(1) Water Particle Velocity around Circular Cylinder

The water particle velocity in the boundary layer must connect with the potential velocity outside the boundary layer that is the water particle velocity of diffracted waves.

Let U, V and W be the water particle velocities of diffracted waves in the direction of the coordinates θ , τ and z respectively. These are determined by MacCamy-Fuchs' velocity potential $\Phi^{[l]}$ as follows:

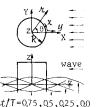


Fig.1 Coordinate

system.

$$u = \frac{1}{n\partial\theta} = \frac{\pi H}{T} \frac{\cosh kh(1+z/h)}{kr \sinh kh} \left[\sum_{n \neq 0}^{\infty} E_n n \left\{ J_n(kr) - \frac{J_n(kr)}{H_n^{(p)}(kr)} \right\} \sin(n\theta) \right] e^{i\sigma t} , \dots (1)$$

$$V = \frac{\partial \Phi}{\partial r} = \frac{\pi H}{T} \frac{\cosh \frac{kh(1+z/h)}{kh}}{\sinh \frac{kh}{kh}} \left[\sum_{n=0}^{\infty} E_n \left\{ J_n(kr) - \frac{J_n(kR)}{H_n^{(2)}(kR)} \right\} \cos(n\theta) \right] e^{i\sigma t} , \cdots (2)$$

$$\mathcal{W} = \frac{\partial \Phi}{\partial z} = \frac{\pi H}{T} \frac{\sinh kh(1+z/h)}{\sinh kh} \left[\prod_{n=0}^{\infty} E_n \left\{ J_n(kn) - \frac{J_n(kR)}{H_n^{(2)}(kR)} H_n^{(2)}(kn) \right\} \cos(n\theta) \right] e^{i\sigma t} , \cdots (3)$$

in which H:wave height, T:wave period, h:water depth, k:wave number, σ :angular frequency, R:radius of cylinder, t:time, J_n , $H_n^{(i)}$ and J_n' , $H_n^{(i)'}$ denote Bessel function of order n, Hankel function of second kind of order n and their derivatives respectively, and $E_0=1$ when n=0 and $E_n=2(i)^n$ when n≥1.

(2) Three Dimensional Laminar Boundary Layer Theory on Circular Cylinder

Using the relations $\theta = x/R$ and $\hbar = R+y$, the Navier-Stokes and continuity equations expressed by the cylindrical coordinates θ , π and z are represented in the boundary layer coordinates x, y and z as follows:

$$\begin{array}{c} u_{t}^{+} \left\{ uu_{x}^{+} uv/R \right\} / \left(1+y/R \right) + vu_{y}^{+} wu_{z}^{-} = \left(1/\rho \right) p_{x}^{-} / \left(1+y/R \right) \\ & + v \left\{ u_{yy}^{+} + u_{y}^{-} / R \left(1+y/R \right) + \left(u_{xx}^{-} - u/R^{2} + 2v_{x}^{-} / R \right) / \left(1+y/R \right)^{2} + u_{zz}^{-} \right\} \\ & w_{t}^{+} uw_{x}^{-} / \left(1+y/R \right) + vw_{y}^{+} uw_{z}^{-} = -g^{-} \left(1/\rho \right) p_{z} \\ & + v \left\{ w_{yy}^{+} + w_{y}^{-} / R \left(1+y/R \right) + w_{xx}^{-} / \left(1+y/R \right)^{2} + w_{zz}^{-} \right\} \\ & u_{x}^{-} \left(1+y/R \right) + v/R \left(1+y/R \right) + v_{y}^{+} w_{z}^{-} \theta \\ & , \end{array} \right\}$$

in which u, v and w denote the water particle velocities in the direction of coordinates x, y and z respectively, and ρ :density, p:pressure, g:accerelation of gravity, v:kinematic viscosity.

Taking $U_{M}=\pi H/T$ as a representative velocity and the wave length $L=2\pi/k$ as a representative length, the quantities containing in Eq.(4) are replaced in the following dimensionless forms:

$$x'=kx, \quad y'=\sqrt{Re}ky, \quad z'=kz, \quad t'=\sigma t, \quad Re=c/\{kv\}, \\ u'=u/u_M, \quad v'=\sqrt{Re}v/u_M, \quad w'=w/u_M, \quad p'=\{p+\rho gz\}/\{\rho c U_M\}, \end{cases}$$

in which C:celerity and Re is a convenient Reynolds number to magnify the coordinate y in the boundary layer. Hereafter, however, for the sake of convenience, dimensionless quantities are denoted without prime.

Rearranging Eq.(4) by substituting Eq.(5), the following dimensionless equations are obtained with respect to dimensionless velocities and pressure, containing the parameters U_M/c , $1/kR\sqrt{Re}$ and 1/Re:

$$\begin{split} u_{t}^{+} (U_{N}/c) \{ (uu_{x}^{+}uv/kR\sqrt{Re}) / (1+y/kR\sqrt{Re}) + vu_{y}^{+}wu_{z} \} \\ &= -p_{x}^{-} / (1+y/kR\sqrt{Re}) + u_{yy}^{+}u_{y}^{-} / \{kR\sqrt{Re}(1+y/kR\sqrt{Re})\} \\ &+ \{u_{xxx}^{-}/Re - u/(kR\sqrt{Re})^{2} + 2v/RekR\sqrt{Re})\} / (1+y/kR\sqrt{Re})^{2} + u_{zz}^{-}/Re , \\ &w_{t}^{+} (U_{N}/c) \{uw_{x}^{-} / (1+y/kR\sqrt{Re}) + vw_{y}^{+}ww_{z}\} \\ &= -p_{z}^{+}w_{yy}^{+}w_{y}^{-} / \{kR\sqrt{Re}(1+y/kR\sqrt{Re})\} + w_{xx}^{-} / \{Re(1+y/kR\sqrt{Re})^{2}\} + w_{zz}^{-}/Re , \\ &(u_{x}^{+}v/kR\sqrt{Re}) / (1+y/kR\sqrt{Re}) + v_{y}^{+}w_{z} = 0 , \end{split}$$

in which $U_M/c=\pi H/L$ is of the order of the wave steepness in magnitude, and is generally supposed to be a very small quantity. Therefore, denoting it by ϵ_1 as

$$\varepsilon_1 = U_M/c = \pi H/L \ll 1$$
,(6)

the dimensionless velocities $u,\; v$ and w are expanded into power series of ϵ_1 as follows:

$$u = u_0 + \varepsilon_1 u_1 + \varepsilon_1^2 u_2 + \cdots, \quad v = v_0 + \varepsilon_1 v_1 + \varepsilon_1^2 v_2 + \cdots, \quad w = w_0 + \varepsilon_1 w_1 + \varepsilon_1^2 w_2 + \cdots + \cdots + (7)$$

Also, $1/kR\sqrt{Re}=\sqrt{\sqrt{1}/2\pi}/R$ is of the order of the ratio of the boundary layer thickness to the radius of cylinder in magnitude, which may generally be very small. Therefore, denoting it by ε_2 as

$$\varepsilon_2 = 1/kR\sqrt{Re} = \sqrt{vT/2\pi/R} \ll 1$$
, $\cdots \approx (8)$

the following approximate series can be introduced:

$$1/(1+y/kR\sqrt{Re})=1/(1+\epsilon_2 y)=1-\epsilon_2 y+\epsilon_2^2 y^2-\cdots$$

In this paper, it is supposed that the order of ϵ_2 in magnitude is the same as ϵ_1 or smaller than ϵ_1 . Moreover, the condition is limited within the range of $kR=2\pi R/L \leqq 1$, and accordingly the order of 1/Re is smaller than that of the square of ϵ_2 since the relation $1/Re=(kR)^2\epsilon_2^{-2}\leqq\epsilon_2^{-2}$ is established.

Then, it is supposed that the velocities outside the boundary layer are represented in terms of the water particle velocities of diffracted waves on the surface of the cylinder obtained by substituting $\pi = R$ into Eqs.(1) and (3). Designating them by U_R and W_R after dividing by U_M , these can be written in the following dimensionless forms:

$$U_{R} = \frac{\cosh(kh+z)}{\sinh kh} \frac{2i}{\pi(kR)^{2}} \left[\sum_{n=0}^{\infty} \frac{n \cdot E_{n}}{H_{n}^{2}(kR)} \sin \frac{nx}{kR} \right] e^{it} , \qquad (10)$$

The dimensionless pressure gradients are approximately expressed by using Eqs.(10) and (11)

By rearranging Eq.(4') with respect to the powers of ε_1 after substituting Eqs.(5) to (11) into Eq.(4'), the first approximate equations concerning ε_1^{0} (order of the zeroth power of ε_1) are obtained as follows:

.

$$u_{0t} - u_{0yy} = u_{R_t} , \quad w_{0t} - w_{0yy} = w_{R_t} , \quad u_{0x} + v_{0y} + w_{0z} = 0 . \quad (13)$$

The boundary conditions are given as

$$y=0: u_0=v_0=w_0=0$$
, $y=\infty: u_0=u_R, w_0=w_R$(14)

The solutions of Eq.(13) satisfying Eq.(14), that is, the first approximate solutions can be obtained in the similar manner to that by Schlichting³⁾, as follows:

$$u_{lst} = u_0 = \zeta_0 (u_0 e^{it}, w_{lst} = w_0 = \zeta_0 (w_0 e^{it}, v_{lst} = v_0 = -\zeta_0 (u_0 + w_0) e^{it}, \dots \dots (15)$$

in which

$$\zeta_{0}^{=1-e^{-(1+i)y/\sqrt{2}}}, \qquad \zeta_{0}^{=y-\frac{1-i}{\sqrt{2}}}\{1-e^{-(1+i)y/\sqrt{2}}\}, \\ U_{0}^{=U_{R}}/e^{it}, \qquad W_{0}^{=W_{R}}/e^{it}.$$

Although U_0 and W_0 are real functions in the case of oscillating flow, they are complex functions in the case of wave motion as recognized from Eqs.(10) and (11). Therefore, the actual water particle velocities are given by the real parts in Eq.(15).

The second approximate equations concerning ϵ_1^{-1} (order of the first power of $\epsilon_1)$ are obtained as

$$u_{1t}^{-}u_{1yy}^{-} \{ u_{R} u_{Rx}^{+} w_{R} u_{Rz}^{-} \} - \{ u_{0} u_{0x}^{+} v_{0} u_{0y}^{-} w_{0} u_{0z}^{-} \} + \{ \varepsilon_{2}^{-} (\varepsilon_{1}^{-}) u_{0y}^{-} , \\ w_{1t}^{-} w_{1yy}^{-} = \{ u_{R} w_{Rx}^{+} w_{R} w_{Rz}^{-} \} - \{ u_{0} w_{0x}^{+} v_{0} u_{0y}^{-} w_{0} w_{0z}^{-} \} + \{ \varepsilon_{2}^{-} (\varepsilon_{1}^{-}) w_{0y}^{-} , \\ u_{1x}^{+} v_{1y}^{-} w_{1z}^{-} = \{ \varepsilon_{2}^{-} (\varepsilon_{1}^{-}) \} \{ g u_{0x}^{-} v_{0}^{-} \} , \end{cases}$$

and the boundary conditions are given by

$$y=0: u_1=v_1=w_1=0$$
, $y=\infty: u_1=0, w_1=0$(18)

Among the solutions of Eq.(17) satisfying Eq.(18), u_1 is described as follows:

$$u_{1} = \{\epsilon_{2}/\epsilon_{1}\} \epsilon_{1}^{i} u_{0} e^{i\sigma t}$$

$$+ \epsilon_{1a}^{i} \{u_{0} u_{0x} + w_{0} w_{0z}\} e^{2i\sigma t} + \epsilon_{1d}^{i} \{u_{0} w_{0z} - w_{0} u_{0z}\} e^{2i\sigma t}$$

$$+ \epsilon_{1b}^{i} \{(\hat{u}_{0} \hat{u}_{0x} + \check{u}_{0} \check{u}_{0x}) + (\hat{w}_{0} \hat{u}_{0z} + \check{w}_{0} \check{u}_{0z})\}$$

$$+ \epsilon_{1c}^{i} \{(\hat{u}_{0} \hat{u}_{0x} - \check{u}_{0} \hat{u}_{0x}) + (\hat{u}_{0} \check{w}_{0z} - \check{u}_{0} \hat{w}_{0z})\}$$

$$+ \epsilon_{1c}^{i} \{(\hat{u}_{0} \hat{w}_{0z} + \check{u}_{0} \check{w}_{0z}) - (\hat{w}_{0} \hat{u}_{0z} + \check{w}_{0} \check{w}_{0z})\}$$

$$(19)$$

in which

$$\zeta_{1}^{\prime} = \frac{1}{\sqrt{2}} \eta^{\prime} e^{-(1+i)\eta^{\prime}} ,$$

$$\zeta_{1a}^{\prime} = \frac{i}{2} e^{-\sqrt{2}(1+i)\eta^{\prime}} + \frac{i}{2} e^{-(1+i)\eta^{\prime}} + \frac{1-i}{2} \eta^{\prime} e^{-(1+i)\eta^{\prime}} ,$$

$$\zeta_{1d}^{\prime} = -\frac{7i}{4} e^{-\sqrt{2}(1+i)\eta^{\prime}} + \frac{3i}{2} e^{-(1+i)\eta^{\prime}} + \frac{1-i}{2} \eta^{\prime} e^{-(1+i)\eta^{\prime}} + \frac{i}{4} e^{-2(1+i)\eta^{\prime}} ,$$

$$(20)$$

$$\zeta_{1b}^{-} = -\frac{3}{4} + \frac{1}{4} e^{-2n'} + e^{-n'} \left(\frac{1}{2} \cos n' + 2 \sin n' \right) - \frac{n}{2} e^{-n'} \left(\cos n' - \sin n' \right) ,$$

$$\zeta_{1c}^{-} = -\frac{3}{4} - \frac{1}{4} e^{-2n'} + e^{-n'} \left(\cos n' - \frac{1}{2} \sin n' \right) + \frac{n}{2} e^{-n'} \left(\cos n' + \sin n' \right) ,$$

$$\zeta_{1e}^{-} = -\frac{1}{2} + e^{-n'} \left(\frac{1}{2} \cos n' + \sin n' \right) - \frac{n'}{2} e^{-n'} \left(\cos n' - \sin n' \right) ,$$

$$(20)$$

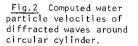
and $n = y/\sqrt{2}$, and \wedge and \checkmark indicate real and imaginary parts respectively. The form of Eq.(19) was identically determined under consideration that the righthand side of Eq.(17) contains the products of complex number, and unknown functions contained in Eq.(19), shown by Eq.(20), were obtained as the sum of homogeneous solution and paticular one, in the same manner as for the first approximate solutions. The second approximate solution of u is indicated by using Eqs.(15) and (19) as

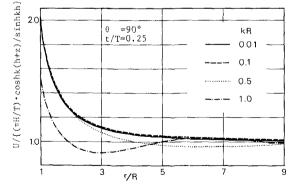
$u_{2nd}=u_0+\varepsilon_1u_1$. (21)

It is recognized that the second approximate solution contains the second harmonic component and the mass transport velocity in addition to the fundamental component. The actual velocity is given by the real part in Eq. (21). ζ_0 , ζ_{1a} and ζ_{1b} are the same as those obtained by Schlichting³, and however, ζ_1 , ζ_{1c} , ζ_{1d} and ζ_{1e} appear as new functions in this study because the boundary layer is treated as three dimensional, the curvature of the circular cylinder is taken into account and the velocities outside the boundary layer are given by the water particle velocities of not oscillating flow but waves.

COMPUTATIONS AND DISCUSSIONS

<u>Fig.2</u> shows the ratio of the water particle velocity of diffracted waves ll calculated by Eq.(1) to the maximum value of the water particle velocity of progressive waves under the condition $\theta=90^{\circ}$ and t/T=0.25. It is found from this figure that the water particle velocity of diffracted waves on the surface of cylinder (t/R=1) is twice as large as the velocity of progressive waves under the condition that the radius of cylinder is small compared with the wave length ($kR_{2}0.5$), and this result corresponds to the theoretical fact that the potential velocity in steady flow³). The velocity decreases rapidly far from the cylinder, and agrees roughly with that of progressive waves under the condition $t/R_{2}5$.





Concerning the velocity profile in the boundary layer, some results of calculation of the second approximation u_{2nd} represented by Eq.(21) are shown. The value of u_{2nd} is determined by giving the values of the following four parameters kh, kR, $\epsilon_1=\pi H/L$ and $\epsilon_2=\sqrt{vT/2\pi}/R$ besides the coordinate variables θ , y/R, z/h and t/T.

Fig.3 shows the variation of the velocity profiles with increase in ε_1 . It is understood from this figure that the more ε_1 increases, the more the difference between u_{2nd} and the potential velocity U_R shown by a broken line increases, and therefore, the connection of u_{2nd} with U_R outside the boundary layer does not become smooth. This is due to the fact that in deriving the second approximation, the boundary condition on the cylinder surface is taken in preference to that outside the boundary layer. If this approximate solution is appropriate, it is expected in the real phenomenon that an abrupt velocity gradient appears in the neighborhood of outside of the boundary layer as the wave height increases, and therefore, small eddies which rotate in the opposite direction to the wake vortex may occur even when the wake vortex does not appear. Such a phenomenon as to support this expectation is seen in <u>Photo.1</u>.

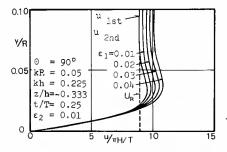


Fig.3 Vatiation of u_{2nd} with ε_1 .



Photo.l Hydrogen bubble lines in boundary layer.

<u>Fig.4</u> shows the variation of the velocity profile with change of ϵ_2 only which is equivarent to change of ν . It is found from this figure that as ϵ_2 increases, the boundary layer thickness increases.

<u>Fig.5</u> shows the variation of the velocity profile with change of the radius of cylinder R only which results in changes of both kR and ε_2 . It is found from this figure that in the case when the radius of cylinder is as small compared with the wave length as kR=0.01, the separation occurs already at $\theta=110^\circ$. In this case, Keulegan-Carpenter's number⁴ (denoted by K.C. hereafter) is

$$K.C. = \frac{U_{max} \cdot T}{2R} = \frac{\pi \varepsilon_1}{kR} \cdot \frac{\cosh kh(1+z/h)}{\sinh kh} = 14.5$$

As mentioned later, even when K.C. is smaller than 14.5, the vortex formation is seen, and therefore, it is reasonable that the separation occurs in this example.

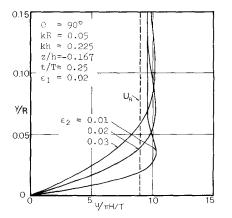
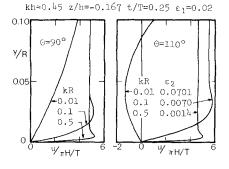


Fig. 4 Variation of u_{2nd} with ε_2 .

 $\frac{\text{Fig.5}}{\text{with } kR \text{ and } \epsilon_2}.$



EXPERIMENTS AND DISCUSSIONS

In order to examine, first of all, the water particle velocity of diffracted waves, a circular cylinder made of Lucite with the radius of 10 cm was installed in the center of the wave tank, which is 17.5m long, 1.5m wide and 75 cm deep. Using a pulse generator, a train of hydrogen bubble lines was generated from a platinum wire with a diameter of 0.1mm stretched horizontally from the surface of the cylinder, and photographs are taken from above the water surface. The sketch of this experimental apparatus is shown in <u>Fig.6</u>.

The platinum wire was painted at intervals of about 1cm so as to recognize the coordinates \hbar and θ of hydrogen bubbles from photographs, an example of which is shown in <u>Photo.2</u>. Thus, the velocities U and V were measured by means of dividing the distances of hydrogen bubbles in the directions of θ and \hbar by the time interval of pulse repeated.

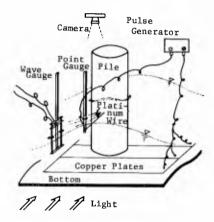
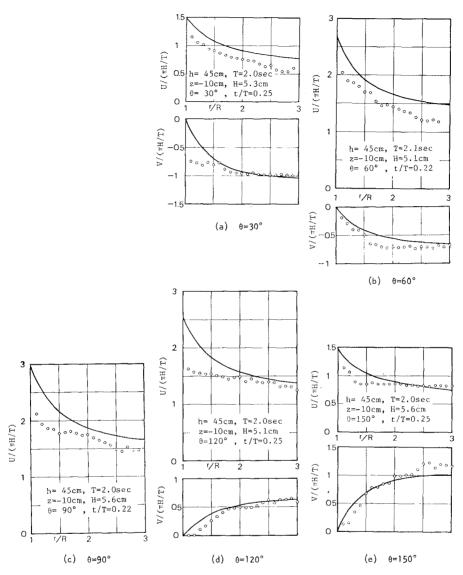


Fig.6 Sketch of experimental apparatus (in case of diffracted waves).



Photo.2 Hydrogen bubble lines of diffracted waves around circular cylinder.

Figs.7 (a)-(e) show comparisons between experimental values of water particle velocities and theoretical curves calculated by Eqs.(1) and (2) denoted by solid lines. It is found from these figures that concerning U, experimental values are generally smaller than theoretical ones, in which both resemble each other in shape in front of the cylinder ($0 < 90^{\circ}$), but differ in rear of the cylinder ($0 > 90^{\circ}$), and that concerning V, both agree roughly. In the analysis of these experimental data, however, it is afraid of containing errors in some extent due to neglecting the change of velocity field in space and time.



 $\frac{Fig.7}{around\ circular\ cylinder\ between\ theory\ and\ experiment.}$

In order to measure the velocity profile in the boundary layer, a semicircular cylinder with a radius of 10cm was attached to the side wall of the wave tank which is 27m long, 50cm wide and 70cm deep as shown in <u>Fig.8</u>, and photographs of hydrogen bubble lines generated from the platinum wire with a diameter of 0.05 mm were taken through the glass bottom.

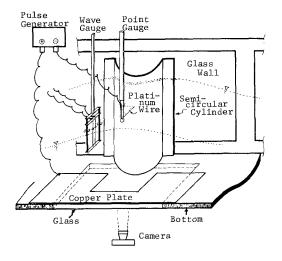


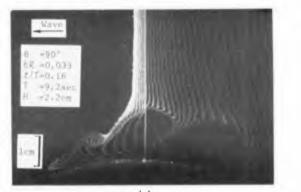
Fig.8 Sketch of experimental apparatus (in case of boundary layer).

The experimental conditions are as follows:

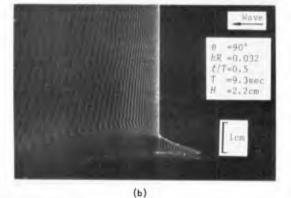
h=45 cm, z=-15 cm, $\theta=90^{\circ}$ and 110° , T:1 to 10 sec, H:1 to 4 cm, $v=1.204\times10^{-2}$ cm²/sec.

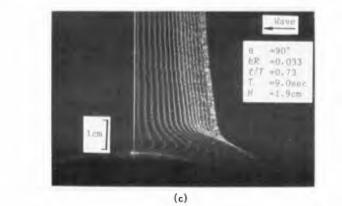
Some examples of the photographs in the boundary layer are shown in <u>Photo.3</u>, and some results of this experiment are shown in <u>Fig.9</u>. In these figures, theoretical velocity profiles of the first and second approximations are also shown by dotted and solid lines respectively. Within the range of the experiment, flow separation were not recognized both in the experiment and the theory. It is found from the figures that measured values are generally smaller than theoretical ones. One of the reasons may be that water particle velocities of diffracted waves in the experiment have a tendency to become smaller than in the potential theory as mentioned above, and in addition, in the boundary layer theory presented in this study, the water particle velocity outside the boundary layer with a finite thickness is given by the value on the surface of cylinder calculated from Eq.(1), which means that the boundary layer thickness is neglected.

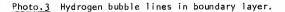
On the other hand, it is recognized from $\underline{Photo.3-(b)}$ or $\underline{Fig.9-(b)}$ that the phase angle of water particle velocities in the boundary layer precedes more than outside the boundary layer.

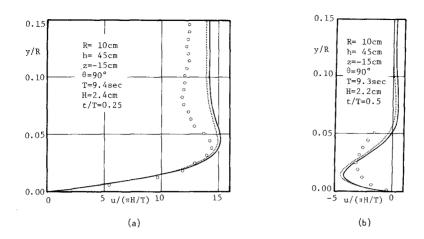












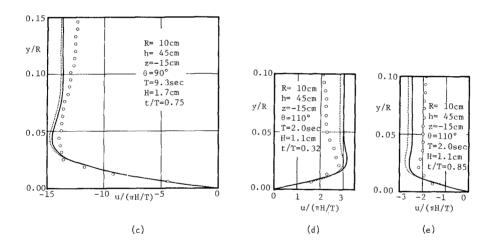


Fig.9 Velocity profiles in laminar boundary layer around circular cylinder due to waves.

Finally, in order to examine the occurrence of wake vortices, photographs were also taken of hydrogen bubble lines produced from the platinum wire stretched in front of a brass pile with a radius of lcm, an example of which is shown in Photo.4.

<u>Fig.10</u> shows a trace of the photograph taken after the wave crest passed over the pile, and <u>Fig.11</u> shows velocity profiles of the second approximation calculated in the same case as in Fig.10. From these figures, the occurrence of laminar flow separation and subsequent development of wake vortices can be recognized. In this case, the location of separation point is derived theoretically as $\theta=102^{\circ}$, which is almost identical to that in steady $flow^{2}$, 3 , and K.C. is equal to 10.7 and the Reynolds number is approximately 1200.

This fact of vortex formation at K.C.=10.7 is consistent with the experimental results obtained by Keulegan and Carpenter⁴). Resently, Sarpkaya investigated experimentally the variation of the drag and inertia coefficients with K.C. in oscillating $flow^{6}$). It is found from his results that at K.C.=12, the drag coefficient reaches to the largest value and the inertia coefficient decreases to the lowest value, which corresponds to the critical condition K.C.=15 obtained by Keulegan and Carpenter⁴). They stated that at K.C.=12.5, a single eddy is formed and is separated during a half cycle of fluid motion, and the process of eddy shedding has a very significant bearing on the variations of the drag and inertia coefficients⁴). Considering their studies, therefore, further investigations are necessary about the time variation of wake vortices under progressive waves.

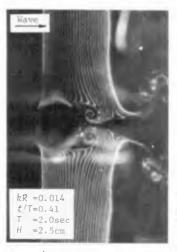


Photo.4 Occurrence of wake vortices behind pile due to waves. (R=1cm)



Fig.10 Occurrence of wake vortices behind pile due to waves.

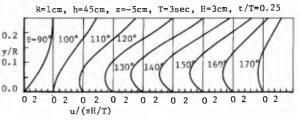


Fig.ll Separation of laminar boundary layer around pile due to waves.

CONCLUSION

In this paper, first of all, the water particle velocities of diffracted waves around a circular cylinder have been discussed, and next, the velocity profiles in the boundary layer on the surface of cylinder have been derived theoretically and compared with the experimental results, and finally, the occurrence of flow separation have been discussed.

Summarizing the results of this study, the following statements are made:

1. Theoretical values of the water particle velocity around a circular cylinder are generally smaller than experimental ones, but both are resemble in velocity profile in front of the cylinder.

2. The second approximate solution of the water particle velocity in the boundary layer explains various characteristics of the boundary layer, that is, boundary layer thickness, precedence of phase angle of water particle velocity in the boundary layer, existence of mass transport velocity in the neighborhood of outside of the boundary layer, and occurrence of flow separation.

3. In order to discuss quantitatively the validity of the second approximate solution, it is necessary to obtain more accurate data, over a wide range, of water particle velocities both in the boundary layer and of diffracted waves.

4. Considering the relationship between flow patterns and wave forces, it is also important to investigate the criterion for flow separation, subsequent vortex formation and vortex shedding under various conditions, and to measure the pressure distribution on the surface of cylinder especially when the wake vortex is formed.

ACKNOWLEDGEMENT

The authors wish to express their gratitudes to Mr. W. Kioka for his assistances through the experiments. This work was partly supported by Scientific Research Funds from the Ministry of Education.

REFERENCES

- MacCamy,R.C., and R.A.Fuchs: Wave forces on piles: Diffraction theory, Tech. Memo., No.69, B.E.B., 1954.
- 2) Chia-Shun Yih: Fluid Mechanics, McGraw-Hill, 1969.
- 3) Schlichting, H.: Boundary Layer Theory, McGraw-Hill, 1968.
- Keulegan, G.H., and L.H. Carpenter: Forces on cylinder and plates in an oscillating fluid, Jour. Res. Nat. Bur. Stand., Vol.60, No.5, pp.423-440, May 1958.
- Iwagaki,Y., H.Ishida and T.Senda: Wave forces on a pile under irregular waves, Proc. 20th Conf. Coastal Eng. in Japan, pp.1-5, Nov.1973. (in Japanese)
- 6) Sarpkaya,T.: Wave forces and periodic flow about cylinder, Summaries of 14th Conf. Coastal Eng., pp.271-274, June 1974.